machines

MDPI

Article

Intelligent Mapping and Control of Stresses in a Hydraulic Materials Handling Crane

Appiah-Osei Agyemang [1], Sasu Mäkinen [1] and Daniel Roozbahani [2,*]

[1] Department of Mechanical Engineering, Lappeenranta-Lahti University of Technology, P.O. Box 20, FI-53851 Lappeenranta, Finland
[2] Department of Electrical and Robotics Engineering, Widener University, One University Place, Chester, PA 19013, USA
* Correspondence: droozbahani@widener.edu

Abstract

The objective of this research was to develop an intelligent stress mapping and a smart control platform, utilizing Artificial Intelligence (AI), to increase the fatigue life of a hydraulic crane. The crane's boom was modeled and co-simulated using ANSYS, ADAMS, and MATLAB. A flexible model of the boom was created in ANSYS and then exported to ADAMS. Stress analysis was performed using the maximum principal hotspot method and the von Mises yield criterion. Stress optimization was conducted using a Neural Network (NN) algorithm, which is a key implementation of AI in this study. Two control platforms, one based on Neural Networks and another on Fuzzy Logic, were designed to apply AI in controlling the crane's movements. The Neural Network algorithm optimized the crane's movement by adjusting velocity at critical positions where structural stress was high, while the fuzzy logic-based control algorithm utilized stress feedback from the crane's structure. Both AI-driven control algorithms were integrated into the physical crane in the lab, and extensive testing demonstrated a significant increase in the crane's fatigue life, along with effective damping of crane vibrations. This paper introduces a novel AI-driven approach combining Neural Networks and Fuzzy Logic for intelligent stress mapping and control, specifically tailored for hydraulic cranes. Unlike previous works, this research integrates real-time stress feedback into the control process and validates the algorithms through experimental implementation on a prototype crane, significantly improving its fatigue life.

Keywords: intelligent control; stress mapping; fatigue life; Neural Network algorithm; fuzzy logic; artificial intelligence in hydraulic crane

Academic Editor: Zheng Chen

Received: 23 April 2026
Revised: 4 June 2026
Accepted: 9 June 2026
Published: 21 June 2026

1. Introduction

Hydraulic cranes, also known as hydraulic booms, utilize hydraulic power to lift and move heavy loads. Comprising a series of interconnected links and components, they enable precise control over the movement of loads, effectively governing their position and/or speed. These cranes have become indispensable in diverse industries such as construction, manufacturing, shipping, forestry, and mining. Their appeal lies in their robustness, adaptability, and capacity to manage heavy loads with minimal inertia, shocks, and vibrations [1-3]. However, given their rigorous operational conditions, the cranes' structural elements are vulnerable to fatigue and stress over time. Such wear and tear can compromise the crane's functionality, structural integrity, and stability, potentially leading to material decay, cracks, or even catastrophic failures [2,4]. While the design of the components of a metal structure for a static loading application is a standardized process, optimizing the fatigue in a metal structure under dynamic loads, where stress levels fluctuate over time, presents significant challenges [5,6]. Consequently, studying the stresses in the components of a hydraulic crane and developing control strategies capable of mitigating the effects of fatigue becomes paramount. Recent innovations in crane controller design, utilizing advanced control methods such as model-based algorithms, adaptive control methods, and intelligent control strategies equipped with powerful optimization algorithms, have significantly enhanced crane precision, efficiency, and reliability. Notable examples include the use of Artificial Intelligence (AI) techniques like Neural Networks (NN), Fuzzy Logic (FL), and Genetic Algorithms (GA) [7-10]. These AI-driven methodologies have enabled more sophisticated control mechanisms that respond intelligently to operational conditions, improving overall performance.

The key research question addressed in this study is: Can intelligent control strategies and utilizing AI techniques effectively optimize stress patterns in hydraulic cranes to extend their fatigue life without compromising performance? This study particularly emphasizes the positive effects of applying AI, specifically Neural Networks and Fuzzy Logic, to the crane's behavior and fatigue life. Neural Networks, with their ability to detect patterns in large datasets, have proven useful in optimizing crane behavior and predicting potential structural failure of the crane's components. However, the performance of the Neural Network algorithm depends heavily on the robustness of the dataset, the training algorithm used, the quality of data, the architecture of the neural network, the training technique, and the available computational resources [11,12]. On the other hand, Fuzzy Logic provides a flexible framework for handling complex and uncertain scenarios, making it ideal for crane control system design. It enables effective pattern recognition of the data extracted from the crane's structure, based on monitoring and analysis using trained algorithms developed from historical data. Fuzzy Logic also plays a crucial role in creating an intelligent optimal controller for the crane, with ease of deployment and transparency in its working process [13-15].

Although many studies have focused on stress analysis in hydraulic cranes and have proposed intelligent control systems, the approach adopted in this study has received relatively little attention. Our aim is to investigate the fatigue patterns in a hydraulic crane and assess the feasibility of using AI-powered intelligent controls to improve its fatigue life. This article also discusses the co-simulation between ADAMS 2023 and MATLAB/Simulink 2022, where the crane was modeled in ADAMS, and its parameters were integrated into MATLAB for co-simulation purposes, enhancing the overall system dynamics. A stress mapping algorithm, driven by a Neural Network, was developed, utilizing the Hot-Spot approximation method and Neural Network-based predictions to forecast stress distribution. Additionally, an intelligent control system was designed to prevent stress-induced fatigue without significantly impacting the crane's operational speed and functionality.

Two AI-based control strategies were developed and implemented: one using a Neural Network algorithm and the other using Fuzzy Logic. These strategies were employed to optimize crane orientation and reduce vibration-induced stress in its structure. The developed control platform optimized the crane's operation by preventing high-frequency vibrations that contribute to fatigue. Moreover, a real-time controller was employed to monitor and minimize stress during crane operation by utilizing data from multiple strain gauges (HBM, Hottinger Brüel & Kjær, Darmstadt, Germany). Movements of the crane's hydraulic cylinders were optimized to the most stress-reducing positions and speeds, minimizing the impact of loads that lead to fatigue. To ensure optimal fatigue life, the crane was tested under various load scenarios. Several operational cycles with different control configurations and parameters were applied to evaluate the effectiveness of the AI-based control algorithms.

The primary contribution of this research lies in the development of a dual AI-based control strategy, applying Neural Networks for stress optimization and Fuzzy Logic for stress feedback control. These contributions represent a notable advancement in intelligent crane control, particularly by integrating real-time experimental validation and demonstrating substantial improvements in fatigue life.

1.1. Literature Review

To date, several studies have investigated the structural fatigue of cranes caused by stresses that occur during operation, as well as the corresponding control performance. In their study, Mikkola [16] investigated the use of ADAMS for dynamic system simulation to obtain the stress history in ANSYS. Rainflow analysis and fuzzy logic were used to estimate the fatigue life, and the results were compared against strain gauge measurements on the physical crane. The authors concluded that the co-simulation methodology involving ANSYS and ADAMS demonstrated high efficiency and accuracy in stress analysis.

Pedersen [17] focused on enhancing the performance of loader cranes beyond current capabilities. The study addressed the fatigue of welded joints and the control of mobile hydraulics, both of which are critical for fatigue-prone welded structures subjected to significant dynamic loading arising from hydraulic actuation. To improve the fatigue performance of welded joints, the study established methods involving post-weld treatment and design optimization, particularly using the notch stress approach tailored to the specific conditions of loader cranes. The study investigated and developed a control scheme to limit dynamic peak loading during crane operation.

Zhidchenko et al. [18] investigated the application of Internet of Things (IoT) and Digital Twin concepts for estimating the fatigue life of hydraulically actuated mobile working machines. Only pressure and position data, acquired during machine operation and processed in the cloud, were used. By combining IoT, digital twin models, and finite element analysis, the authors proposed an approach for calculating the stress history and estimating fatigue life.

Zhao et al. [19] studied the establishment of fatigue models to accurately predict the residual fatigue cycles and estimate the service life of a remanufactured excavator using an S-N curve, rainflow counting algorithm, and FEA model. The total stress cycles were calculated using Miner's linear cumulative damage rule, and the results improved the accuracy of estimating the residual service life of the remanufactured excavator beam, thereby enhancing reliability and safety.

The study by Buczkowski and Żyliński [4] focused on performing a finite element fatigue analysis of an unsupported crane and on evaluating its structural integrity and fatigue life under various loading conditions. Using the finite element analysis software ABAQUS, the authors simulated and analyzed the stress distribution and fatigue damage accumulation in the crane's components, highlighting critical areas prone to fatigue failure.

Hectors et al. [20] explored the application of fracture mechanics and hot spot stress-based approaches to estimate the fatigue life of a crane runway girder and identify critical areas prone to fatigue failure. The study focused on assessing the structural integrity and durability of the girder under cyclic loading conditions and provided a basis for optimizing its design and maintenance strategies.

Li et al. [21] investigated the dynamic impact on cranes during the lifting process and developed a dynamic model to examine load variations in crane structures, motivated by the limitations of conventional quasi-static load methods in accurately predicting the fatigue life of cranes. A fatigue life prediction method that considers the lifting impact effect was proposed to analyze structural fatigue life and the lifting impact process.

Recent studies have also advanced neural-network-based and robust control of hydraulic systems, achieving high-accuracy motion tracking and strong robustness to parameter uncertainty and disturbances [22,23]. These works focus primarily on the precise nd robust control of the actuator motion. In contrast, the present work targets the reduction in structural stress and the extension of the fatigue life of the crane: the AI controllers are driven by the structural stress state, mapped offline by a Neural Network and measured online by a strain gauge, rather than by a motion-tracking error, and the approach is validated experimentally on a physical crane. The proposed method is therefore complementary to these motion-oriented controllers and could be combined with them, using a robust or neural-network-based motion controller for accurate tracking together with the proposed stress-based restriction for fatigue mitigation.

1.2. Hydraulic Crane Under Study

The hydraulic crane under study is illustrated in Figure 1 [24]. The crane is securely mounted on a stand, which is itself firmly fixed to the concrete floor of the laboratory hall. This construction ensures a friction-locked connection, preventing any swerving or deviation from the crane's original position, thereby maintaining its precise and stable placement. The crane is constructed from FE-510 steel (specifically grade S355) and has a maximum load capacity of 1080 kg and a maximum reach of 7.2 m. The crane comprises mechanical links, joints, a tank, a pump, filters, various types of valves, a double-acting cylinder with a diameter of 100 mm and a piston diameter of 15 mm, and a hydraulic boom measuring 4125 × 100 × 150 mm.

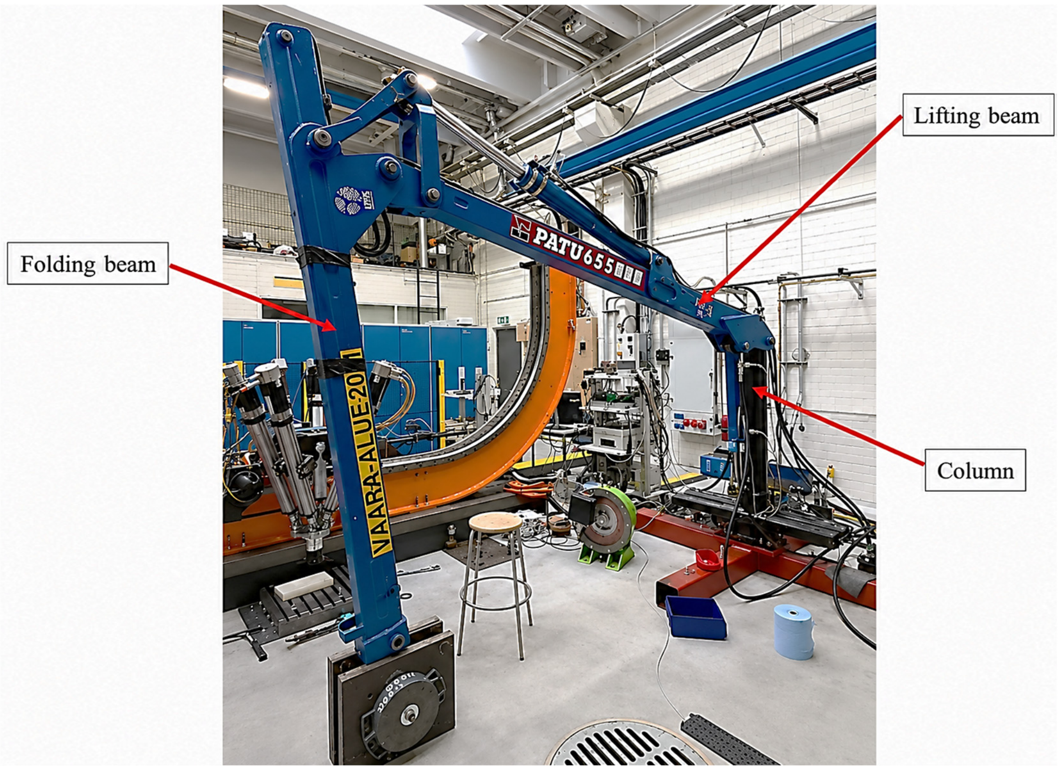

Figure 1. The hydraulic loader crane studied in this work (PATU-655, Kesla Oyj, Joensuu, Finland).

2. System Modeling

To capture the factors that govern the behavior of the crane, a simulation model was developed. The crane model was initially created in SolidWorks 2022 and subsequently imported into ADAMS, a widely used Multibody Dynamics (MBD) software, to incorporate various joints and consider hydraulic components within the ADAMS model. Schematic diagrams of full and simplified models of the crane, pillar, beam, hydraulic cylinder, and piston modeled in SolidWorks are shown in Figure 2.

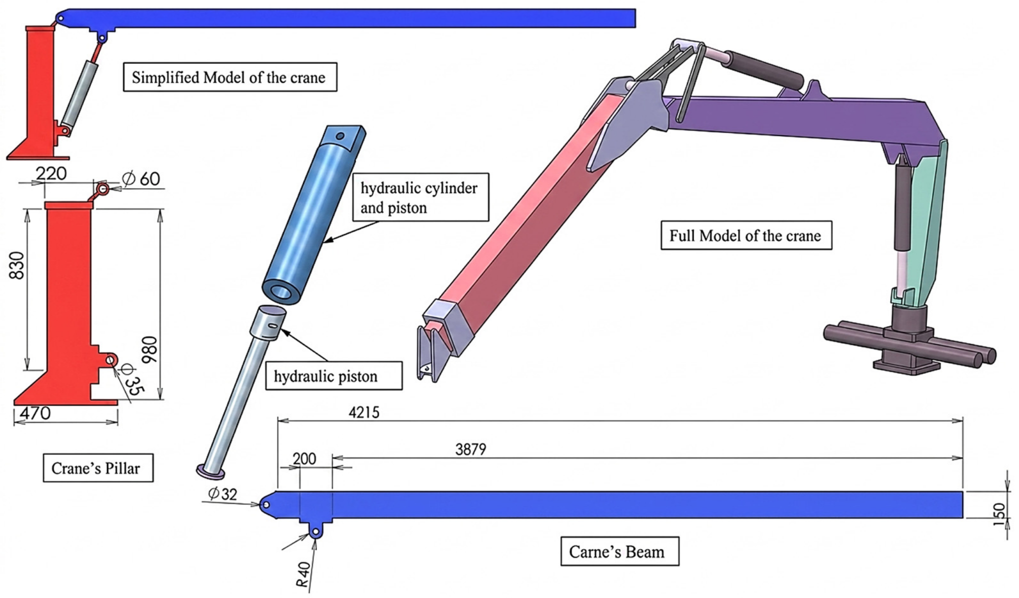

Figure 2. Full and simplified models of the crane, pillar, beam, cylinder, and piston were modeled in SolidWorks.

Mathematical Model

Figure 3 illustrates the diagram of a double-acting hydraulic actuator.

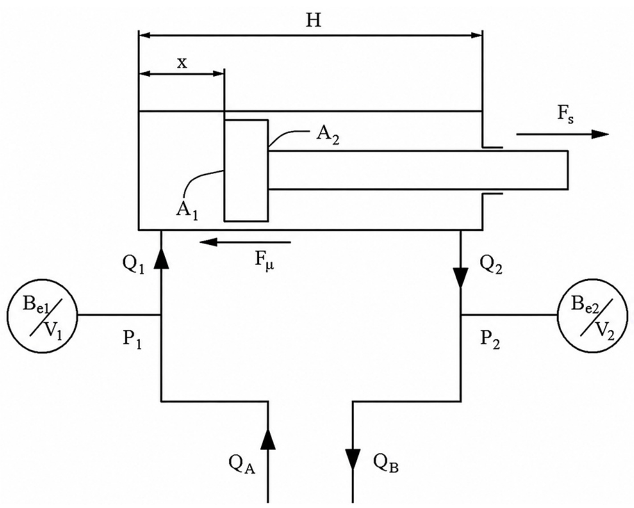

Figure 3. Schematic of the double-acting hydraulic cylinder that actuates the boom.

The force generated by the actuator is formulated by Equation (1):

$$F_S = (p_1 A_1 - p_2 A_2) - \sum F\mu \quad (1)$$

where p_1 and p_2 are the pressures on the piston and piston-rod, A_1 and A_2 are the areas of the piston and piston-rod, and $F\mu$ is the total friction force caused by sealing.

https://doi.org/10.3390/machines14060709

The attenuation of cylinder oscillations is predominantly governed by the frictional force arising from the interaction between the seal material and the cylinder wall. The hydraulic friction force can be described as the resultant of the pressure differential across the piston chambers and the piston's velocity, formulated by Equation (2). This factor significantly contributes to the suppression of vibrations within the cylinder.

$$F\mu = \xi(\dot{x})(p_1 A_1 - p_2 A_2)(1-\eta) \quad (2)$$

where ξ ($\dot{x}$) is the coulomb friction function, and η is the efficiency factor.

Volume flows are generated by the motion of the cylinder, which can be formulated as Equation (3):

$$\begin{aligned} Q_1 &= A_1 \dot{x} \\ Q_2 &= A_2 \dot{x} \end{aligned} \quad (3)$$

where Q_1 and Q_2 are the incoming and outgoing volume flow rates of the cylinder, and $\dot{x}$ is the piston velocity.

The pressure (P) within a hydraulic volume can be mathematically described as a function of the effective bulk modulus (B_e), the volume (V) of the hydraulic system, and the incoming and outgoing flows. This relationship can be expressed through the utilization of a differential equation, which is represented as Equation (4):

$$\begin{aligned} \dot{p_1} &= \frac{B_{e1}}{V_1 + xA_1}(Q_A - Q_1) \\ \dot{p_2} &= \frac{B_{e2}}{V_2 + (H-x)A_2}(Q_2 - Q_B) \end{aligned} \quad (4)$$

where $Q_A - Q_1$ and $Q_2 - Q_B$ is the sum of incoming and outgoing flows related to volume V_1 and V_2, respectively, H is the length of the cylinder, and x is the piston position.

3. Co-Simulation

Co-simulation involves combining multiple simulation tools to simulate different aspects of the system simultaneously [25,26]. Co-simulation between ADAMS and MATLAB/Simulink was performed in this study, the schematic of which is shown in Figure 4 [27].

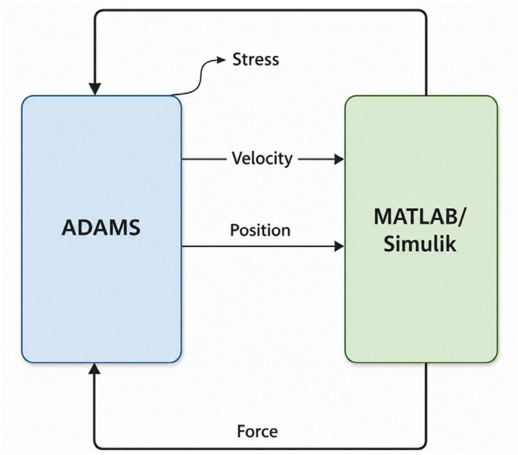

Figure 4. Co-simulation architecture coupling the ADAMS multibody model with the MATLAB/Simulink control model.

The integration of the ADAMS block into the MATLAB/Simulink platform is accomplished automatically as part of the control system. The control system incorporates a proportional-integral-derivative (PID) controller, and the specific initial parameter values employed for the control system were determined as $Kp = 20$, $Ki = 0.2$, and $Kd = 0$ to exhibit excellent performance. The positions, velocity, pressures, and hydraulic force results are illustrated in Figures 5–10.

https://doi.org/10.3390/machines14060709

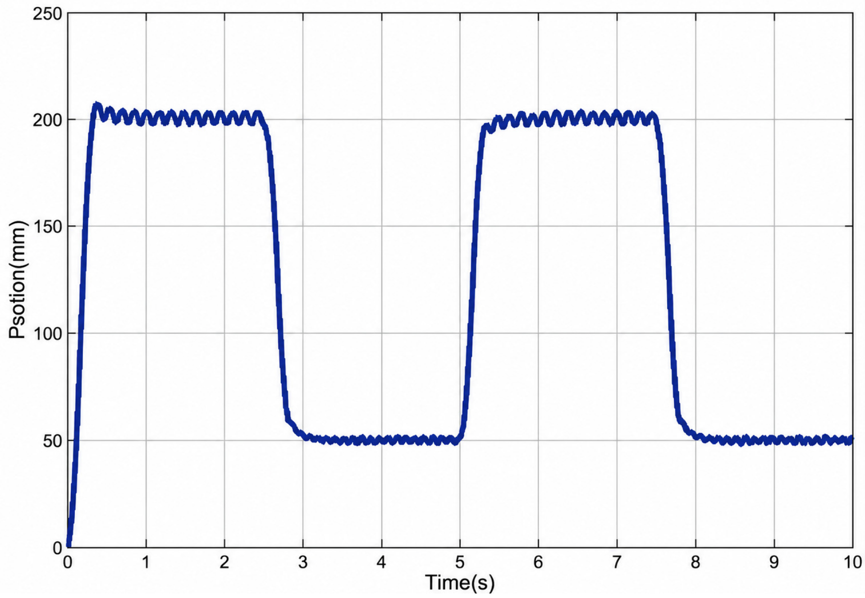

Figure 5. Position response of the hydraulic actuator obtained from the Simulink co-simulation.

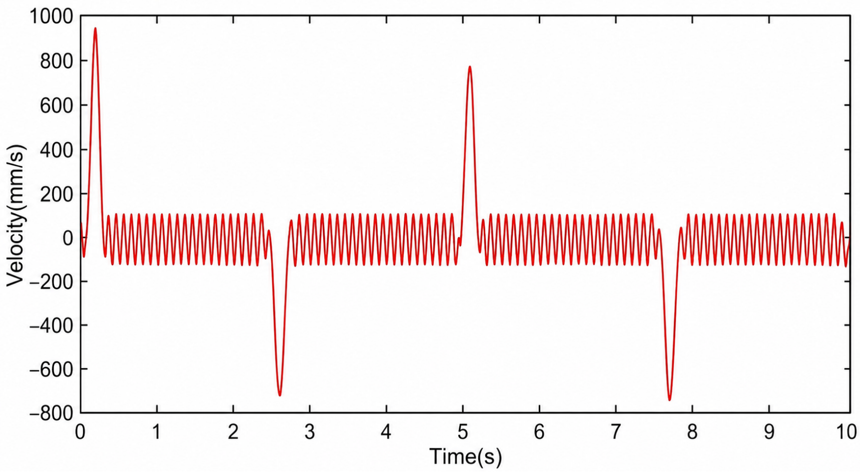

Figure 6. Velocity of the hydraulic actuator obtained from the co-simulation.

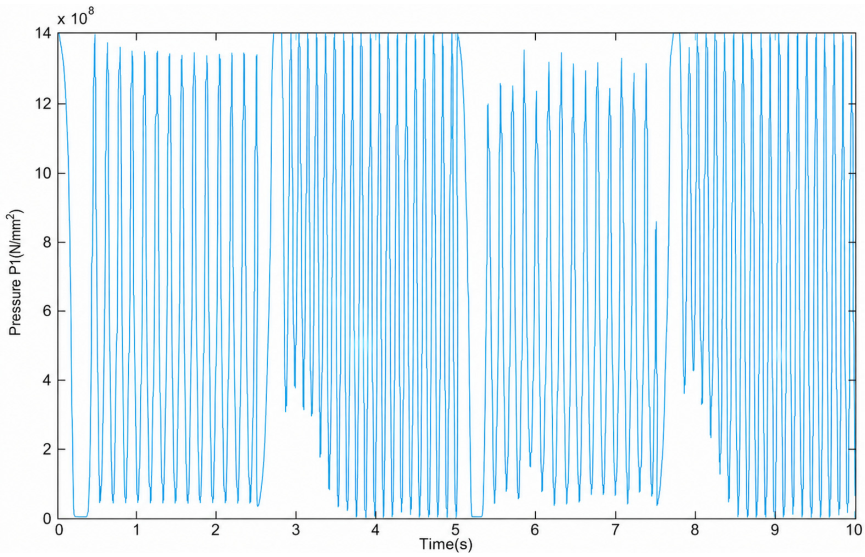

Figure 7. Simulated pressure P_1 in the piston-side chamber of the hydraulic cylinder.

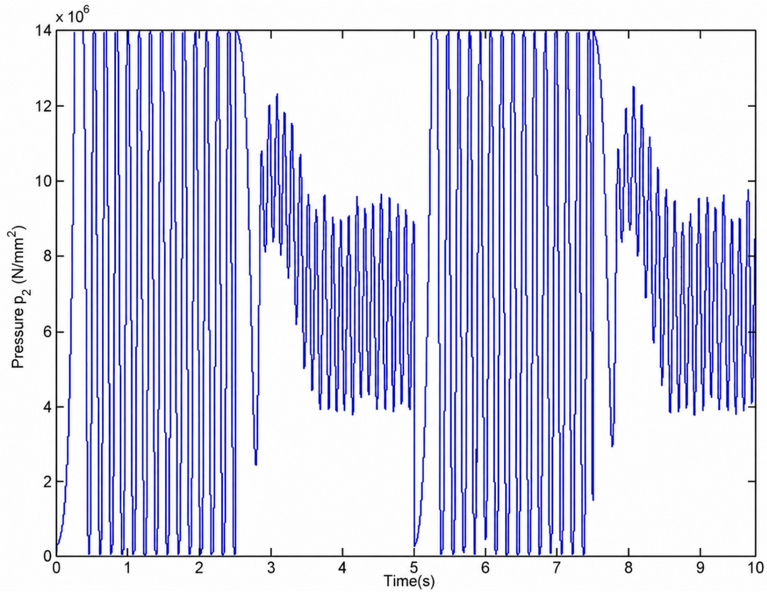

Figure 8. Simulated pressure P_2 in the rod-side chamber of the hydraulic cylinder.

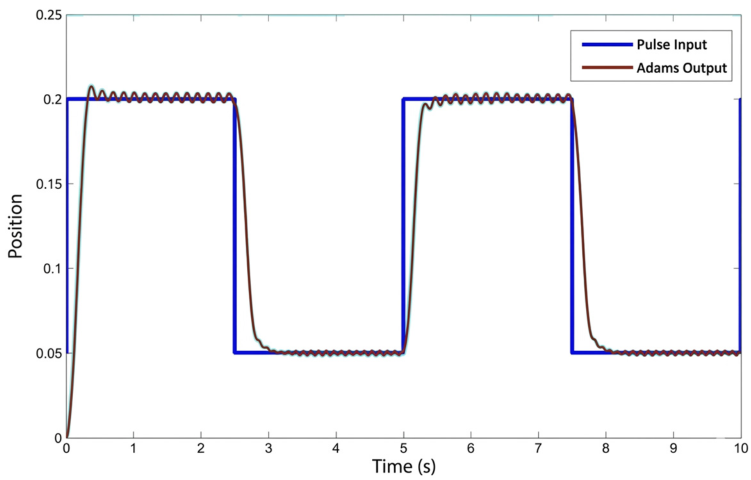

Figure 9. Track of the commanded pulse position input by the simulated piston under PID control.

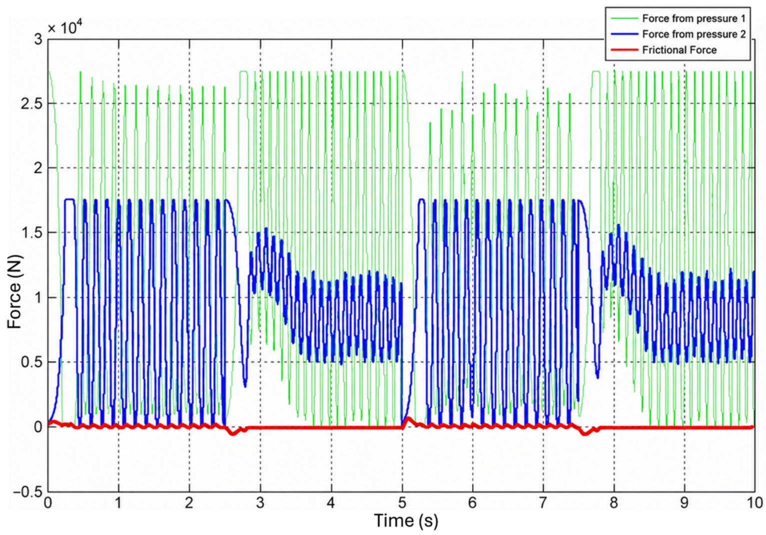

Figure 10. Hydraulic forces acting on the piston during the cycle: the forces generated by chamber pressures P_1 and P_2 and the friction force.

4. Stress Analysis

The stress analysis of the crane is highly influenced by the flexibility of the boom. Various methods can be used to obtain the flexibility of the boom [28,29]. The most accurate stress analysis can be achieved using the finite element method (FEM). However, FEM imposes significant computational demands [30,31]. In this study, two different approaches were employed to address the flexibility of the boom.

In the first method, the SolidWorks model was transferred to ANSYS 2021 software to evaluate the boom's flexibility prior to incorporating it into the ADAMS model. Strain gauges were applied to marked points on the real boom, and these points were measured and modeled as nodes in ANSYS. Owing to computational limitations, only a subset of nodes (approximately 100) was used in ANSYS, as employing the complete set of nodes was not feasible. ANSYS generated a finite element model of the boom using ADAMS macros, which required a modal neutral file (MNF file) containing information about the flexibility of the body. A fine meshing technique was employed to ensure accurate results. Key points along the central axis were established to generate corresponding nodes with six degrees of freedom. Specifically, two nodes were created to accommodate the dual joints or hinges of the boom. Subsequently, all the nodes were selected to generate the output neutral file of the boom. The modal neutral file (MNF) was then exported directly to the ADAMS software. In the second method, the flexibility of the boom was directly assessed within ADAMS. In ADAMS, flexible bodies were created by converting rigid bodies into MNF-based flexible bodies. The flexible body can be directly created using discrete links in the model, which contains essential information such as material type, number of segments, damping ratio, and cross-section details. The created flexible beam in ANSYS and ADAMS is illustrated in Figure 11 [27].

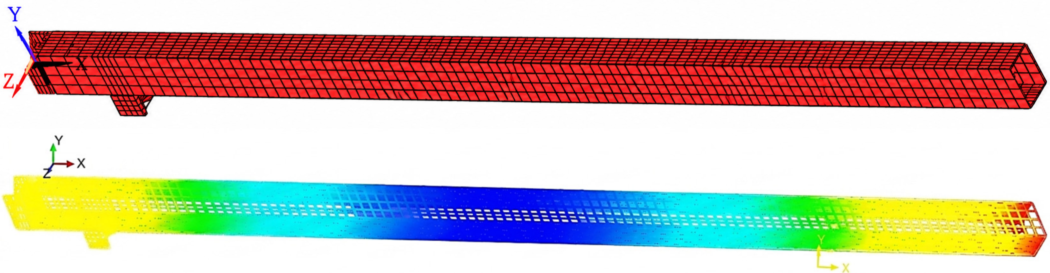

Figure 11. Flexible model of the lifting boom: (**top**) the finite-element mesh generated in ANSYS and (**bottom**) the corresponding discrete-link flexible body in ADAMS. The colors are produced by the default model rendering and do not represent any physical quantity such as stress.

The structural stress and its fatigue life are influenced by material properties, geometric characteristics, and loading parameters. The hot spot stress method is recognized for its efficiency and its ability to provide a straightforward distribution of structural stress [32,33]. In this approach, the critical location with the highest stress concentration is identified in the crane. This method is primarily used when the weld of interest is subjected to nearly perpendicular varying stresses, and the crack can be assumed to originate from defects within the weld. The method is particularly valuable when the detail under consideration does not correspond to any of the known cases covered by the nominal stress method. The approach has been incorporated into the European standard SFS-ENV 1993-1-1 [34] and the latest IIW recommendations. The method determines the hot spot stress, which includes the effects of both macro geometric and structural discontinuities. The hot spot stress can be measured from a prototype, calculated from a Finite Element (FEM) model, or estimated from nominal stress variations. In this study, the stresses were obtained through co-simulation in ADAMS and from the real crane in the laboratory. The

https://doi.org/10.3390/machines14060709

data collected from the laboratory experiments were used both to train the model and to validate the co-simulation model. Table 1 presents the top ten hot spots calculated based on maximum principal stress. The highest hot spot for maximum principal stress occurred at node 480, with a corresponding value of 113.133 MPa. Figure 12 shows the simulated maximum principal stresses [27].

Table 1. Ten Hot Spots based on the maximum principal stresses.

MAXIMUM PRINCIPAL Hot Spots for Boom_flex						
Model = model_1		**Analysis = Last_Run**		**Time = 0 to 9.99999 s Radius = 10.0 mm Location with respect to LPRF (mm)**		
Hot Spot #	**Stress (N/mm²)**	**Node Id**	**Time (s)**	***x***	**Y**	**z**
1	113.133	480	0.0058651	427.98	75	12.5
2	109.168	483	0.0058651	543.45	75	12.5
3	104.674	481	0.0058651	466.47	75	12.5
4	103.494	488	0.0058651	735.9	75	12.5
5	101.899	482	0.0058651	504.96	75	12.5
6	100.532	587	0.0058651	735.9	75	25
7	100.339	485	0.0058651	620.43	75	12.5
8	99.3179	486	0.0058651	658.92	75	12.5
9	97.7697	582	0.0058651	543.45	75	25
10	97.2961	585	0.0058651	658.92	75	25

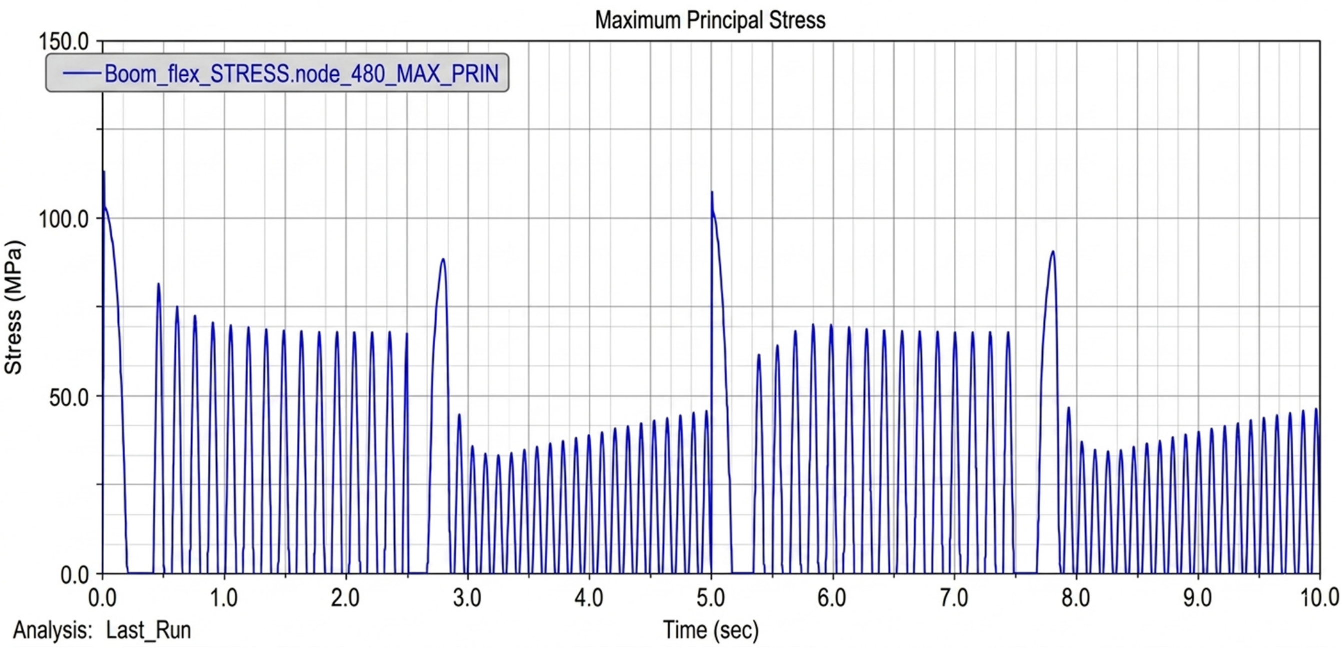

Figure 12. Simulated maximum principal stress history at the most critical hot-spot node (node 480).

The von Mises yield criterion was also utilized for stress analysis, and the ten hot spots for von Mises stresses were analyzed [35,36]. The maximum hot spot von Mises stress was estimated as 112.546 MPa. Table 2 presents the calculated values for the ten hot spots for von Mises stresses, and Figure 13 illustrates the simulated results for the hot spot Von Mises Stresses. Notably, the maximum hot spot for von Mises stress was lower than the maximum principal stress, with values of 112.546 MPa and 113.133 MPa, respectively. The maximum von Mises stress was selected for further analysis in the neural network because the boom is made of steel, a ductile material. The principal stresses were considered unsuitable, as they are less appropriate for ductile materials.

https://doi.org/10.3390/machines14060709

Table 2. Ten Hot Spots for the Von Mises stresses.

VON MISES Hot Spots for Boom_flex						
Model = model_1		Analysis = Last_Run		Time = 0 to 9.99999 s Radius = 10.0 mm Location with respect to LPRF (mm)		
Hot Spot #	**Stress (N/mm²)**	**Node Id**	**Time (s)**	**X**	**Y**	**Z**
1	112.546	2296	0.0058651	2044.56	75	−12.5
2	105.031	480	0.00670297	427.98	75	12.5
3	104.164	483	0.0058651	543.45	75	12.5
4	98.7443	482	0.0058651	504.96	75	12.5
5	98.6352	481	0.0058651	466.47	75	12.5
6	95.5754	2395	0.0058651	2044.56	75	−25
7	91.9115	488	0.0058651	735.9	75	12.5
8	91.8243	485	0.0058651	620.43	75	12.5
9	89.8302	486	0.0058651	658.92	75	12.5
10	89.5118	582	0.0058651	543.45	75	25

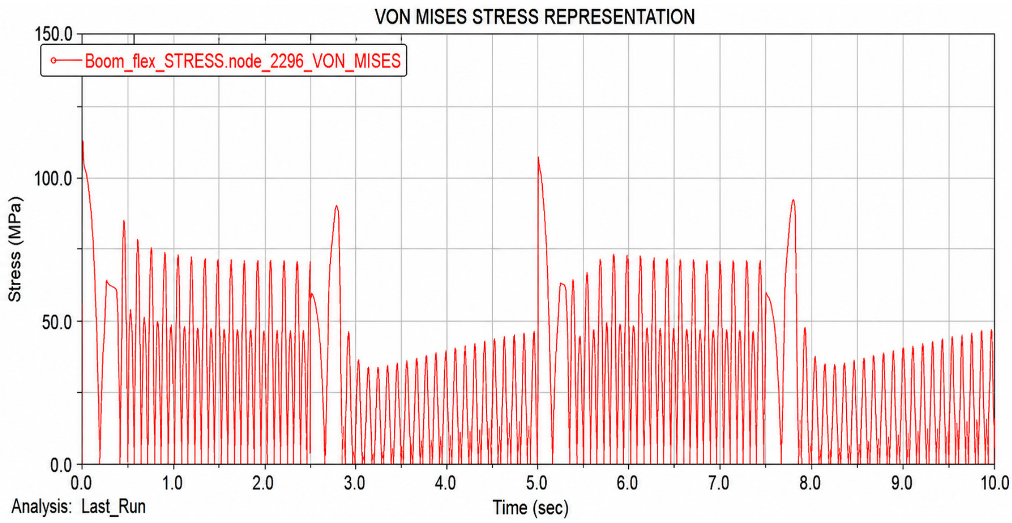

Figure 13. Simulated von Mises stress history at the most critical hot-spot node (node 2296).

Based on these stress analyses, the critical location with regard to potential fatigue was identified as the area depicted in Figure 14. This particular location experiences the highest principal stresses during different operation cycles. In addition, the selected region of the lifting boom, which is frequently examined, contains welded hydraulic pipe fixtures that introduce stress concentrations and fatigue-prone initiation sites for cracks. The stress histories obtained from simulations depict the nominal normal stresses along the longitudinal axis of the boom at the analysis point.

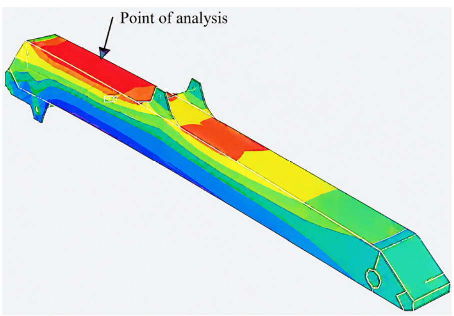

Figure 14. Von Mises stress distribution over the lifting boom obtained from the FE analysis. The color scale indicates the magnitude of the von Mises stress; from blue (lowest) to red (highest).

https://doi.org/10.3390/machines14060709

Based on the performed stress analysis, a stress optimization process was also carried out. A neural network (NN) was used for this purpose. Following the successful training of the neural network using the hot spot approximation demonstrated in Figure 15, the Neural Network training error and its convergence are displayed in Figure 16, and the results presented in Figures 17 and 18 were obtained. In Figure 18, a comparison is made between the von Mises stress generated by an ADAMS model and the estimated approximation of hot spot stress using a Neural Network. The efficacy of the network's training is evident from the obtained results. The regression analysis evaluating the predictive capability of the network is shown in Figure 19.

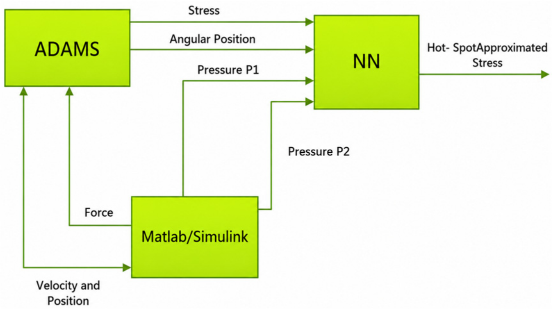

Figure 15. Architecture of the Neural Network (NN) used to approximate the hot-spot stress.

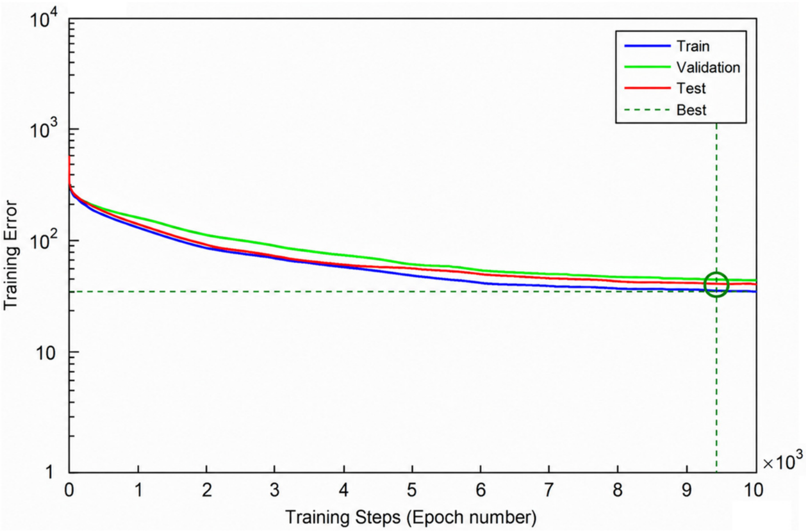

Figure 16. Training Convergence, Validation, and Test Errors of the feed-forward back-propagation.

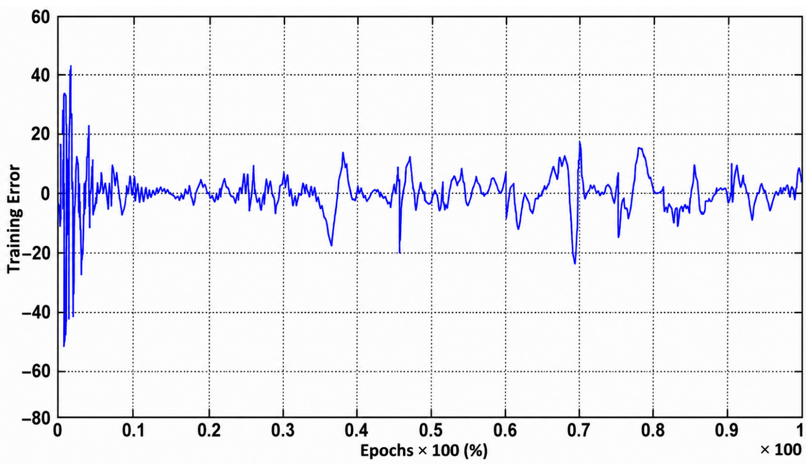

Figure 17. Neural Network training error (residual between the predicted and target stress).

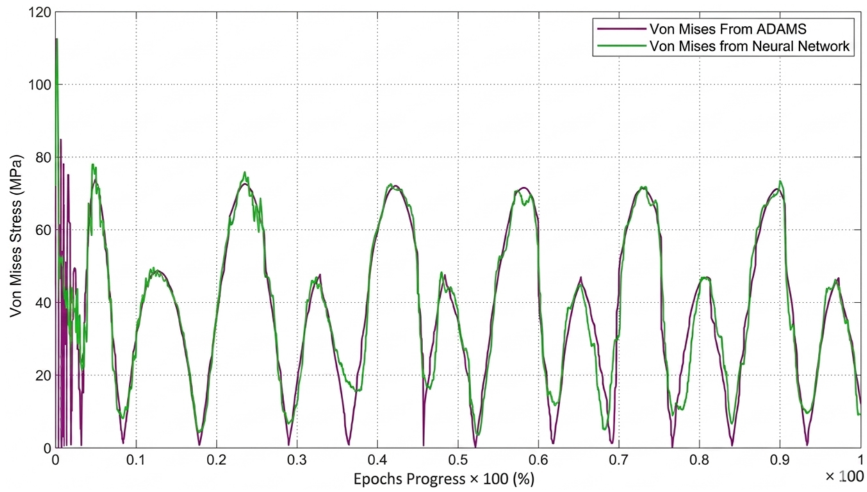

Figure 18. Comparison of the von Mises stress computed by the ADAMS model with the hot-spot stress predicted by the trained Neural Network.

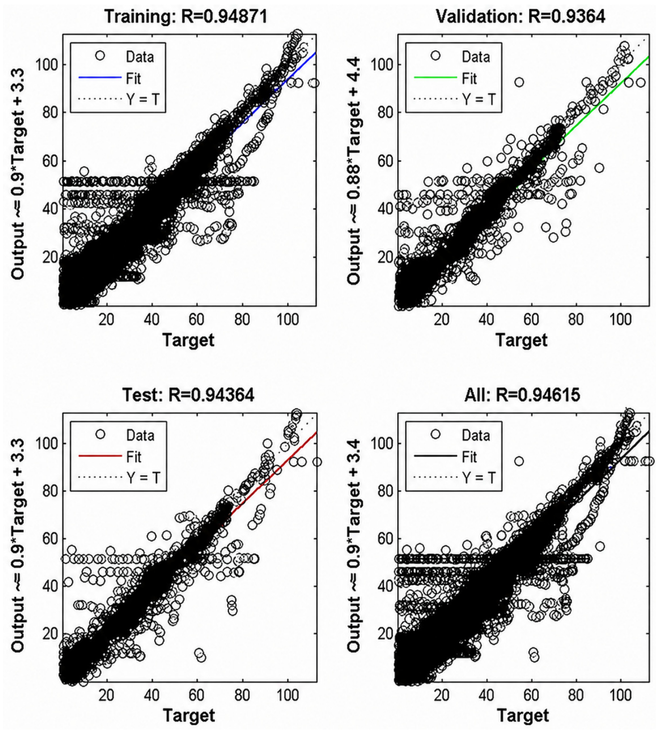

Figure 19. Regression of the trained Neural Network outputs against the target stresses for the training, validation, test, and combined data sets (correlation coefficient R ≈ 0.95).

The Neural Network used for this stress approximation was a three-layer feed-forward network trained with the back-propagation algorithm. Its inputs were the quantities provided by the co-simulation, namely the crane angular position, the chamber pressures P1 and P2, and the cylinder velocity, position, and force shown in Figure 15, and its single output was the corresponding hot-spot stress. The network was trained in MATLAB on the data generated by the validated ADAMS co-simulation; the dataset was divided into training (70%), validation (15%), and test (15%) subsets, and the number of hidden neurons was chosen by gradually increasing it until the validation error no longer improved. Training was performed for 10,000 epochs by minimizing the mean-squared error, and the trained network was tested both against the von Mises stress of the ADAMS model (Figure 18) and against the strain-gauge measurements obtained from the physical crane, reaching a regression coefficient of approximately 0.95 (Figure 19).

5. Control Algorithms

Another aim of this study was to explore the applicability of intelligent control systems for improving the fatigue life of the crane. The intelligent controller should protect the boom from vibration-induced stresses that lead to fatigue while minimally affecting the crane's normal performance. The influence of the control system on operating efficiency was an important consideration during its development. Therefore, the control algorithm was programmed to engage selectively within a specific operational range, where the resultant loads exert a substantial impact on fatigue life. This design approach aimed to minimize the incidence of elevated stress peaks in the stress history. Neural network (NN) and fuzzy logic were applied as intelligent control systems in this study and were implemented through two distinct approaches. In the first method, the command to the valve is restricted according to the orientation of the crane; in the second, it is restricted or modified according to the prevailing stress state in the lifting boom. These algorithms can also be integrated to exploit the advantages of both approaches.

These two AI strategies are complementary and were combined deliberately. The Neural Network controller is a feed-forward, anticipatory scheme that learns the position–stress relationship offline and limits the valve signal according to the crane orientation, so it is effective even without a real-time stress sensor, but it depends on the coverage of the training data. The fuzzy-logic controller is a reactive, feedback scheme that uses the real-time measured stress, is transparent and easy to deploy, and handles uncertainty well, but its action against sudden stress spikes is limited by the valve response speed. Using only the Neural Network would forgo the real-time stress feedback, whereas using only the fuzzy controller would forgo the anticipatory, position-based limitation; combining them allows the system both to anticipate the fatigue-critical postures and to react to the measured stress state. The overall real-time control procedure is summarized in Algorithm 1.

Algorithm 1. AI-based stress-limiting control of the hydraulic crane

Input: operator reference signal u_ref; crane orientation (lifting and folding cylinder lengths); measured stress; reference stress; trained Neural Network; fuzzy inference system; maximum restriction level u_lim (2.3 V or 2.5 V).

Output: applied valve control signal u.

```
for each control step do
   measure the crane orientation and the stress from the strain gauge
   c: = NN(orientation)   // criticality coefficient between 0 and 1
   u_max_NN: = c-scaled value of u_lim   // orientation-based restriction
   d: = measured stress - reference stress
   u_max_FL: = FIS(u_ref, d)   // boundary value from the fuzzy surface
   u_max: = min(u_max_NN, u_max_FL)   // either or both branches may be enabled
   u: = min(u_ref, u_max)   // limit the operator command
   apply u to the lifting-cylinder valve
end for
```

5.1. Orientation Feedback Control

The first method, orientation feedback control, restricts the control signal sent to the valves according to the crane's position. This reduces the volumetric flow through the valve at sensitive positions, lowering the velocities of the crane's cylinders and the resulting actuation forces, and thereby limiting the stresses caused by inertial effects.

A neural network was used to restrict the control signal because of its ability to handle large datasets effectively. The training data for the neural network were generated from the simulation model by dividing the motion ranges of the lifting and folding cylinders into 20 segments. The corresponding static solutions for each combination of the cylinder lengths were calculated, the results of which included the cylinder stroke lengths and the stress values at the selected point of interest. Thus, the influence of the crane's position on the resulting stress states was determined. The resulting stress values were

https://doi.org/10.3390/machines14060709

scaled to coefficients ranging from 0 to 1, representing the criticality of each crane position, and were used as training data for a three-layer feedforward perceptron network. The magnitude of the coefficient as a function of the crane's position is shown in Figure 20, where the surface represents the values produced by the neural network from the independent inputs and the circles denote the measured points from the training data. By amplifying or reducing the coefficient generated by the neural network, relative to the maximum attainable value of the control signal, the upper limit of the control signal is determined. The simulation model of the controller was implemented using MATLAB/Simulink.

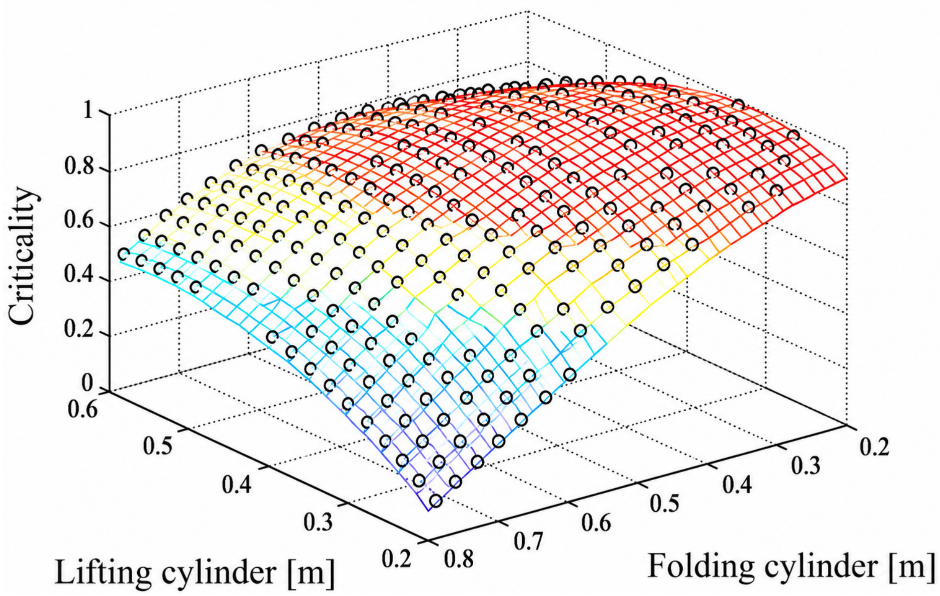

Figure 20. Stress-based criticality coefficient as a function of the lifting- and folding-cylinder lengths (crane orientation). The surface color indicates the magnitude of the criticality coefficient (from low to high), and the circles denote the measured training points.

The stress value computed at each crane position was normalized by the maximum stress obtained over the entire operating range, so that the most fatigue-critical position takes the value 1 and the least-loaded position approaches 0; this criticality coefficient is therefore equivalent to a normalized stress (load) factor that expresses the relative severity of each posture. The Neural Network does not perform any online optimization: it is a feed-forward network, trained offline, that returns this coefficient for the current orientation, and the upper limit of the valve control signal is obtained by scaling the maximum attainable valve signal by the coefficient. The values 2.3 V and 2.5 V denote the two maximum restriction levels that were evaluated, and not the output of an optimization algorithm. The purpose of the Neural Network is thus to provide, in real time and directly from the crane orientation, the precomputed stress information used to limit the valve signal, thereby reducing the cylinder velocity and the inertial loading in the fatigue-critical positions while avoiding a costly online stress computation.

The valve opening restriction based on the crane's orientation was tested during an operation cycle, where the crane followed the work sequence depicted in Figure 21. In the first movement of the operation cycle, the lifting cylinder is used to raise the lifting boom to an upright position. Next, the folding cylinder is engaged to rotate the folding boom to approximately a 90-degree angle relative to the lifting boom. After that, the lifting cylinder is used to lower the lifting boom. Finally, the folding cylinder is activated to unfold the folding boom outward.

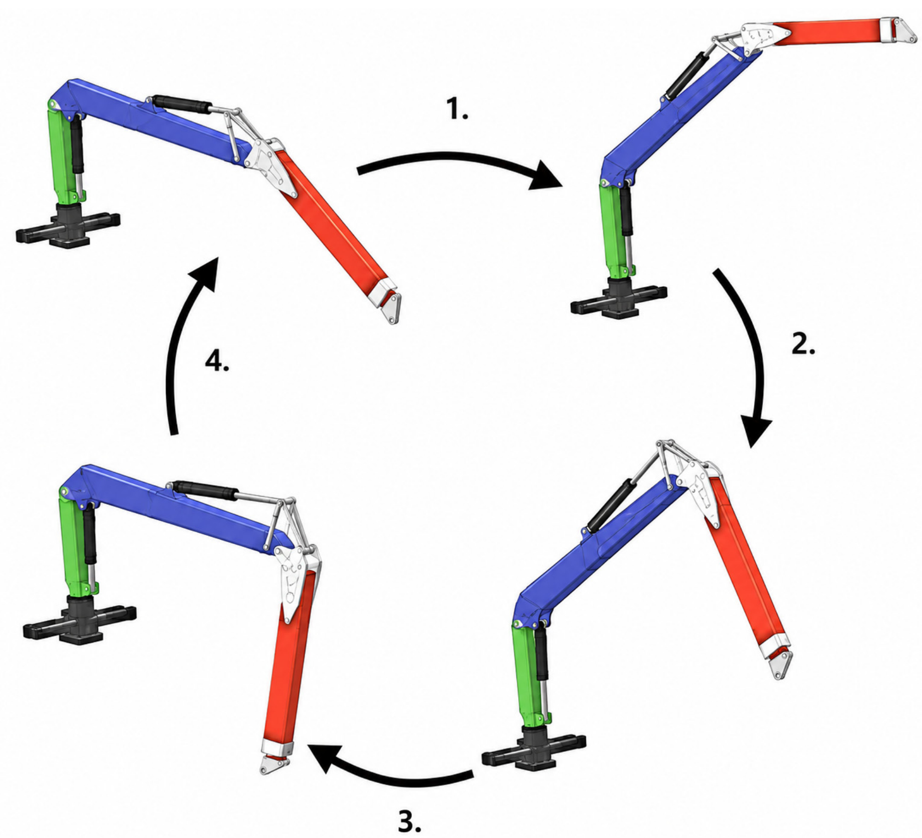

Figure 21. The simulated operation cycle: (1) the lifting cylinder raises the lifting boom; (2) the folding cylinder rotates the folding boom to about 90°; (3) the lifting cylinder lowers the lifting boom; and (4) the folding cylinder unfolds the folding boom. The column, lifting boom, and folding boom of the crane are shown in green, blue, and red, respectively.

The functionality of the controller was confirmed by the increased rise time of the cylinder stroke resulting from the restricted valve opening and by the reduced crane vibrations during the stopping phase, as shown in Figure 22.

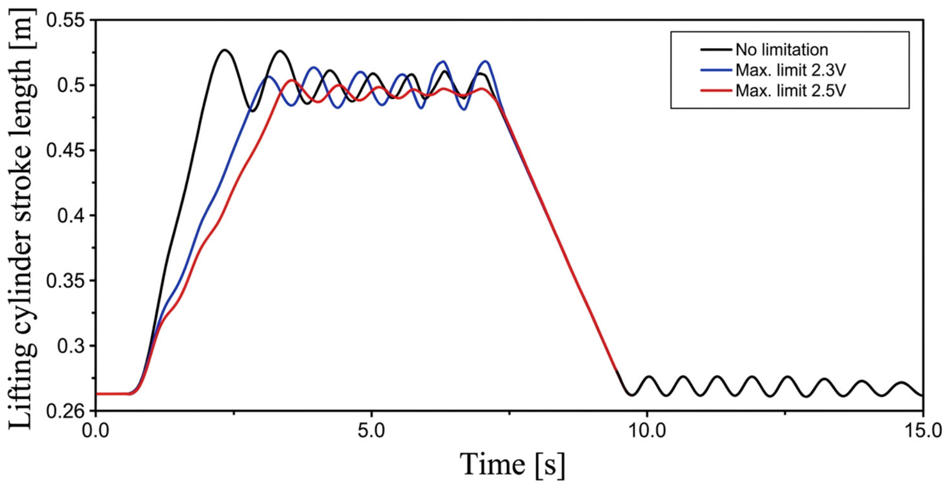

Figure 22. Stroke length of the lifting cylinder over the operation cycle without control and with the orientation-based (NN) controller at maximum valve-signal restrictions of 2.3 V and 2.5 V.

The extent of the opening limitation, the maximum value of the valve's control signal, and the period required for the valve to achieve the desired position are evident in the control signal fed to the valve, as presented in Figure 23.

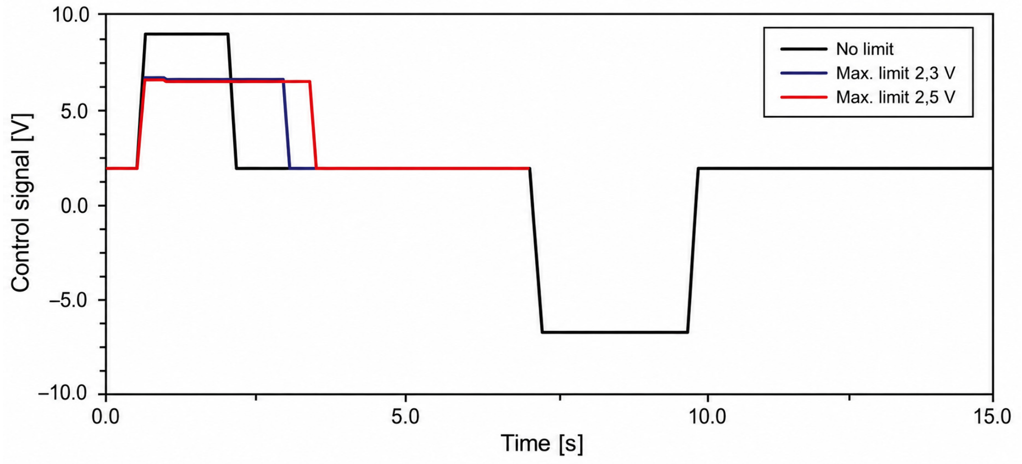

Figure 23. Control signal applied to the lifting-cylinder valve over the operation cycle for the unrestricted case and for the orientation-based controller at maximum restrictions of 2.3 V and 2.5 V.

Throughout the operation cycle, the stress history at the selected point follows the pattern shown in Figure 24, which demonstrates that the controller reduces the vibration-induced stresses that lead to fatigue. To evaluate the magnitude of this effect, constant amplitude equivalent stress variations were calculated from the stress histories, resulting in the values presented in Table 3.

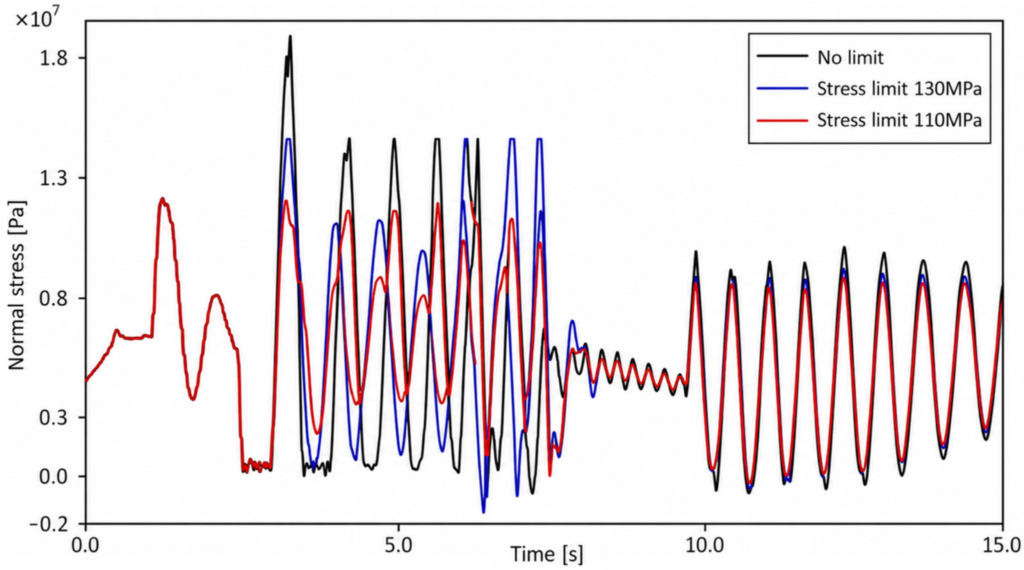

Figure 24. Stress history at the selected critical point over the operation cycle without control and with the orientation-based (Neural Network) controller.

Table 3. Equivalent stress fluctuations.

Max Valve Control Signal Restriction	Equivalent Stress Fluctuation [MPa]
No restriction	89.6
2.3 V	72.9
2.5 V	56.5

The influence of the controller on the fatigue life was assessed using the characteristic fatigue life, obtained by comparing the equivalent stress fluctuation with the FAT 103 Wöhler curve using a Ks value of 10 [37]. In Table 4, the fatigue life refers to the number of repetitions of the previously presented operation cycle.

Table 4. Impact on Fatigue Life.

Max Valve Control Signal Restriction	Fatigue Life (Repetitions)	Fatigue Life Amendment
No restriction	3,100,000	
2.3 V	5,900,000	%90
2.5 V	12,200,000	%290

It should be noted that these results are specific to this particular operation cycle. In practice, however, the distribution of the crane's motion trajectories is such that a large proportion of load lifting and lowering operations occurs within this region.

5.2. Stress Feedback Control

In the second approach, the controller responds in real time to the stress state in the lifting boom, measured using a strain gauge. The difference between the stress measured by the strain gauge and the reference stress is fed into a fuzzy logic system, which determines the maximum control signal applied to the valve. Fixed-value membership functions were used to determine the output, yielding the control surface shown in Figure 25. The controller was then simulated during the previously presented operation cycle, during which the stroke length of the lifting cylinder follows the pattern in Figure 26. It is evident from the lifting cylinder's stroke length that the control algorithm has a damping effect on crane vibrations.

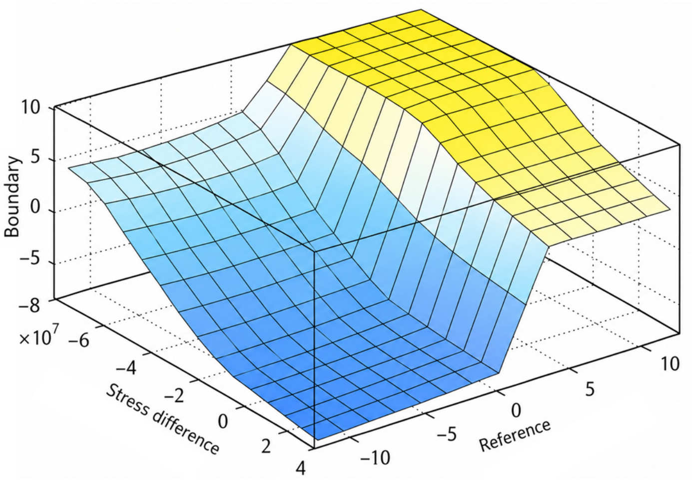

Figure 25. Control surface of the fuzzy-logic stress-feedback controller. The surface color indicates the magnitude of the boundary value, i.e., the maximum permitted valve control signal.

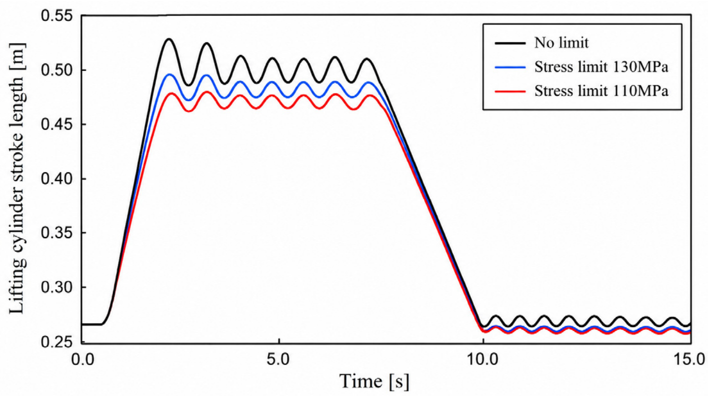

Figure 26. Stroke length of the lifting cylinder over the operation cycle without control and with the fuzzy stress-feedback controller at stress limits of 130 and 110 MPa.

The fuzzy controller has two inputs, namely the operator reference (command) signal and the stress difference (the strain-gauge stress minus the reference stress), and one output, namely the upper limit of the valve control signal. Fixed-value (singleton) output membership functions were used, and the rule base was defined heuristically from the physical relationship between the stress difference and the required restriction, so that the permitted control signal is progressively reduced as the measured stress approaches or exceeds the reference value, whereas at low stress, the command is passed through essentially unaltered. Evaluating this rule base over the full input ranges produces the control surface in Figure 25, in which the two horizontal axes are the reference signal and the stress difference, and the vertical axis (boundary) is the resulting maximum permitted value of the valve control signal.

The effect of the developed algorithm on the control signal fed to the valve is illustrated in Figure 27. The objective was to return the stress state to a satisfactory level. However, the performance of the stress feedback control was limited by the use of a valve that could not respond quickly enough to sudden stress spikes. During the simulated operation cycle, the stress history at the selected point follows the pattern depicted in Figure 28, demonstrating the effect of the developed algorithm on the occurrence of loads that lead to fatigue.

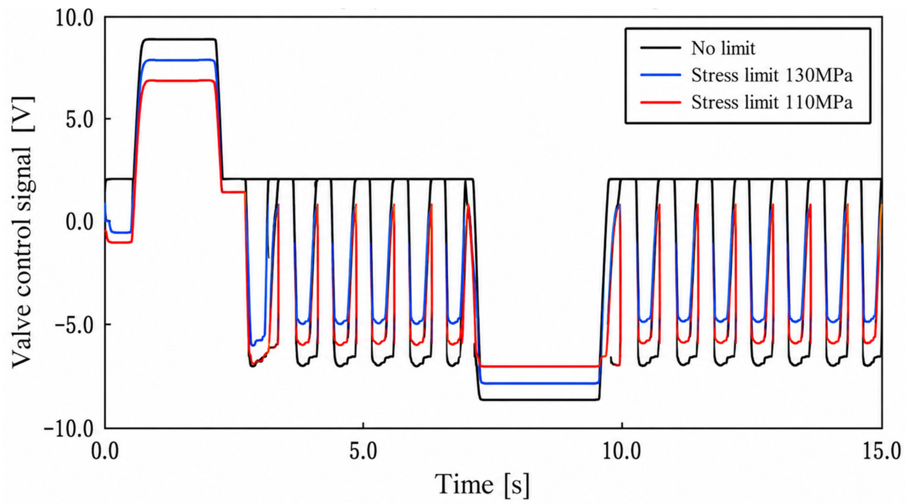

Figure 27. Reference signal applied to the lifting-cylinder valve over the operation cycle for the unrestricted case and for the fuzzy stress-feedback controller at stress limits of 130 and 110 MPa.

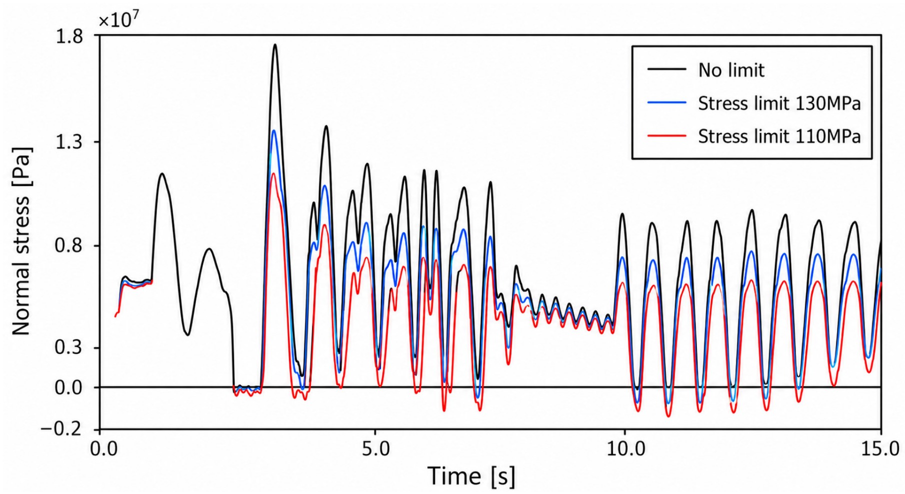

Figure 28. Normal stress at the observation point over the operation cycle without control and with the fuzzy stress-feedback controller at stress limits of 130 and 110 MPa.

https://doi.org/10.3390/machines14060709

The constant-amplitude stress ranges calculated from the stress history using the rainflow algorithm are summarized in Table 5.

Table 5. Equivalent constant amplitude stress fluctuations.

Controller	Equivalent Stress Fluctuations
No restriction	89.6 MP
130 MPa stress restriction	71.0 MP
110 MPa stress restriction	66.3 MP

By calculating the fatigue life according to FAT 103 with a Ks of 1.0 and comparing the cases, the effect of the controller on the fatigue life can be estimated, as shown in Table 6 [37].

Table 6. Fatigue life estimates.

Controller	Cycles of Fatigue Life	Amendment
No restriction	3,060,000	
130 MPa stress restriction	6,130,000	%100
110 MPa stress restriction	7,520,000	%146

6. Experimental Results

Multiple test cycles were performed in laboratory conditions with varying controller parameters to evaluate the performance of the control algorithms. Since the crane's operation cycles predominantly involve short reaches, whereas the most damaging loads occur at longer reaches, the effect of the controller across the entire operating range and over the full fatigue life was investigated by dividing the crane's operating range into four segments, as illustrated in Figure 29; the actual effect of the control algorithm was then assessed by weighting these segments in the fatigue life calculations.

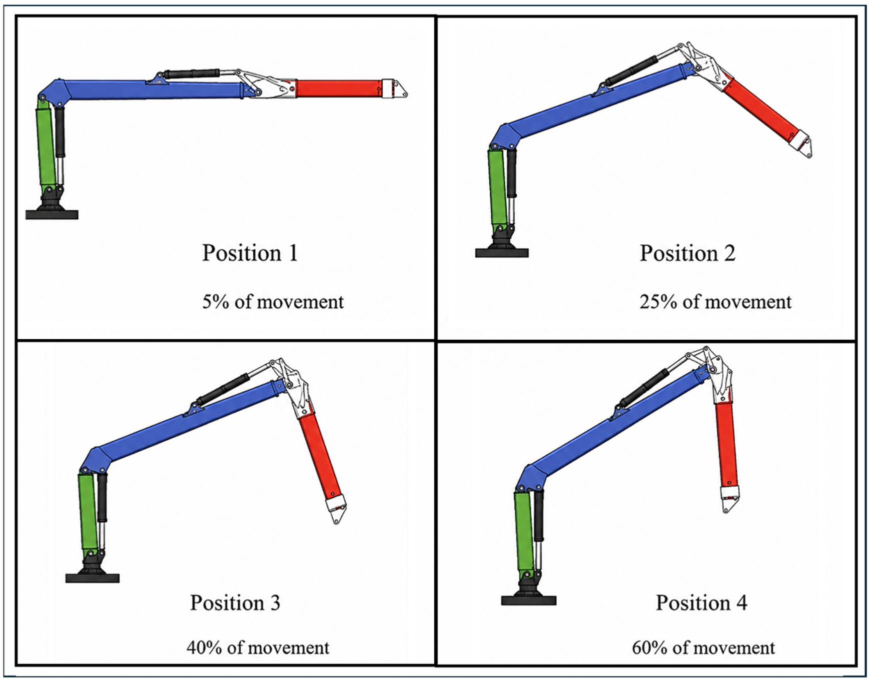

Figure 29. Division of the crane's operating range into four representative postures (Positions 1–4, corresponding to 5%, 25%, 40%, and 30% of the movement range) is used to weight the controller's effect in the fatigue-life assessment. The column, lifting boom, and folding boom are shown in green, blue, and red, respectively.

The stroke of the lifting cylinder was according to Figure 30, with the reference signal fed to the valve of the lifting cylinder shown in Figure 31 for each position.

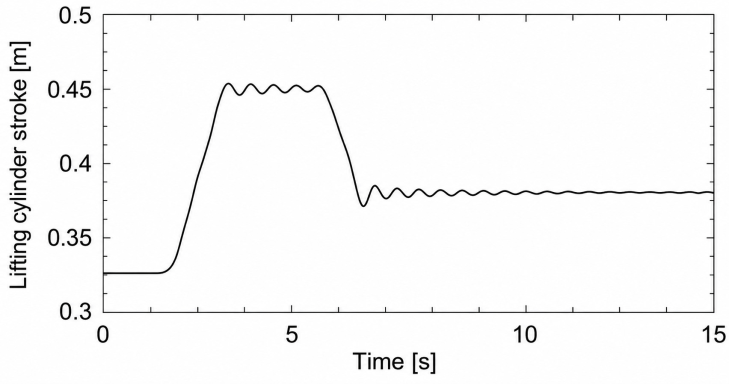

Figure 30. Measured stroke of the lifting cylinder during the experimental test operation cycle.

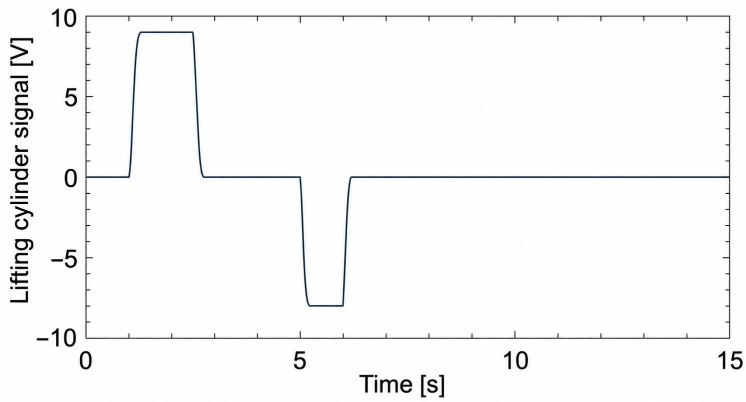

Figure 31. Reference signal applied to the lifting-cylinder valve during the experimental test operation cycle.

The stress history measured from the strain gauge on the lifting boom is shown in Figure 32. The influence of post-movement vibration on the resulting stress fluctuations can be observed in the figure.

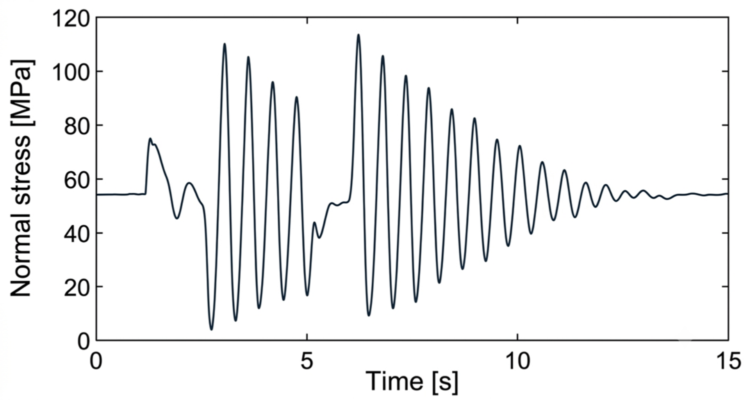

Figure 32. Stress history measured by the strain gauge on the lifting boom.

To evaluate the performance of the controller, the previously presented test operation cycle was executed with the controller's parameters as listed in Table 7 [37]. Constant-amplitude equivalent stress ranges were calculated from the measured stress histories and are presented in Table 8.

Table 7. Test parameters.

Test Run	Reference Limitation	Stress Limit
1	0	-
2	Max. 2.0	-
3	Max. 2.5	-
4	0	130 MP
5	0	110 MP
6	Max. 1.5	120 MP
7	Max. 1.5	110 MP

Table 8. Equivalent stress range calculated from operation cycles.

Trial	Posture 1	Posture 2	Posture 3	Posture 4
# 1	62.01	59.39	50.34	30.49
# 2	51.52	47.04	46.01	30.03
# 3	44.83	37.44	39.94	33.68
# 4	51.32	38.4	38.7	31.29
# 5	38.54	33.16	30.58	24.54
# 6	41.16	34.6	31.69	24.59
# 7	35.64	32.47	27.21	22.58

The reduction in fatigue life caused by the welded hydraulic pipe attachments on top of the lifting boom was also taken into account using the nominal stress method, in accordance with the SFS 2378 [38] standard, with a VL of 80, yielding the values shown in Table 9.

Table 9. The effect of the controller on fatigue life.

Trial	Reference Limit	Stress Limit	Cycles of Work Life	Fatigue Life Variation Compared to Trial 1.
# 1	0 V	-	8,270,000	
# 2	Max. 2.0 V	-	12,809,000	%55
# 3	Max. 2.5 V	-	18,764,000	%127
# 4	0 V	130 MP	19,216,000	%132
# 5	0 V	110 MP	36,769,000	%345
# 6	Max. 1.5 V	120 MP	32,998,000	%299
# 7	Max. 1.5 V	110 MP	45,850,000	%454

However, reducing the fatigue loads alters the dynamic characteristics of the crane, and constraining the valve reference reduces the flow rate through the valve, thereby slowing the motion in the regions that are most exposed to the loads that cause fatigue. This effect can reduce the performance of the crane in the fully horizontal position. However, since this position seldom occurs in practice, the reduction in motion velocity may have little impact when the crane's operation is considered across its entire operational range. Figure 33 illustrates the effect of test run 3 on the crane's motion in the most critical position, which indicates that the motion of the lifting cylinder decelerates. The maximum speed of the lifting cylinder was recorded from the test operation cycles described above in order to quantify the reduction in motion speed. The highest lifting cylinder velocities during lifting motions are presented in Table 10. As the results show, the maximum velocities of the lifting cylinder in the most critical position decreased compared with the normal control. However, it should be noted that this decrease in velocity does not significantly impact the overall operational efficiency.

https://doi.org/10.3390/machines14060709

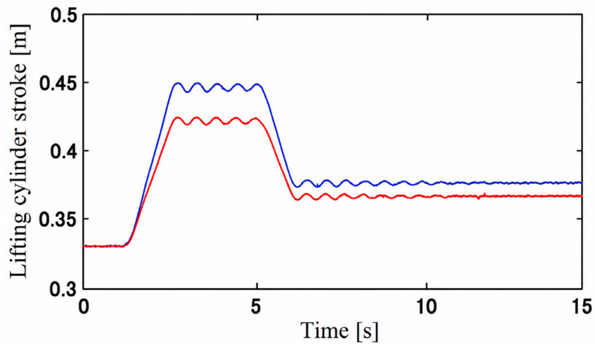

Figure 33. Effect of the controller on the stroke length of the lifting cylinder in the most critical position (test run 3). The blue and red lines denote the traditional and the developed controller, respectively.

Table 10. Maximum lifting cylinder velocities in the course of lifting movements.

Trial	Reference Limit	Stress Limit	Lifting Velocity	Lifting Velocity
# 1	0	-	Max. 0.0837 m/s	Max. 100.0%
# 2	Max. 2.0	-	Max. 0.0645 m/s	Max. 77.1%
# 3	Max. 2.5	-	Max. 0.0556 m/s	Max. 66.4%
# 4	0	130 MP	Max. 0.0836 m/s	Max. 99.9%
# 5	0	110 MP	Max. 0.0823 m/s	Max. 98.3%
# 6	Max. 1.5	120 MP	Max. 0.0735 m/s	Max. 87.8%
# 7	Max. 1.5	110 MP	Max. 0.0739 m/s	Max. 88.3%

In stress-feedback control, the driver's instruction to the valve remains unchanged until the stresses approach the critical range set by the system, which also ensures that the velocities are preserved, as seen in Table 10. Usually, the highest stress peaks occur when the crane's movement is being halted. In such instances, the controller opens the valve to reduce the stress peaks, which also dampens the crane's vibrations, as illustrated in Figure 34. The stroke of the lifting cylinder operated with the traditional controller and with the developed controller is indicated by the blue and red lines, respectively.

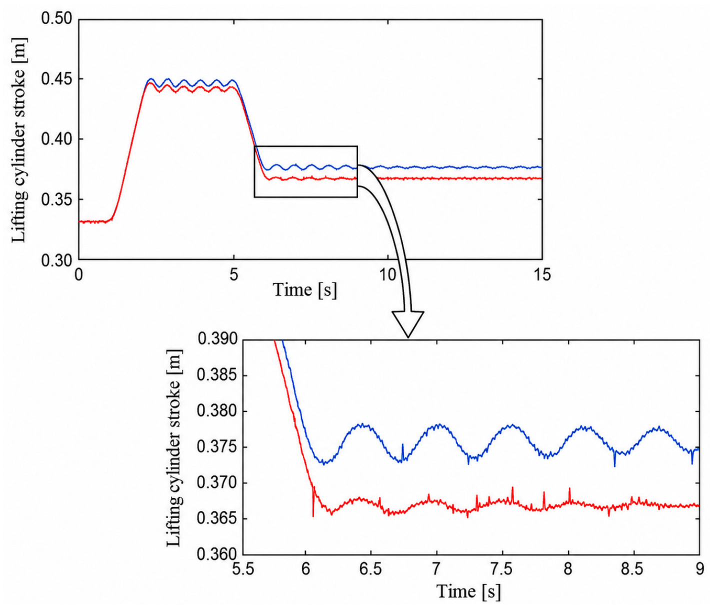

Figure 34. Effect of the controller on crane vibrations during the stopping phase: stroke of the lifting cylinder with the traditional and the developed controllers. The blue and red lines denote the traditional and the developed controller, respectively.

One notable limitation of stress feedback control is a slight tendency toward load creep when stopping, which is somewhat greater than with traditional controllers. This behavior is illustrated in Figure 34, where a small positional error can be observed in the cylinder length after the movement has ceased.

To evaluate the damping of the vibrations, the y-position of the crane's bucket was calculated from the measured cylinder lengths in Figure 34. The vibration sample taken in the time interval of 6.2–8.2 s was analyzed using FFT (Fast Fourier Transform) to calculate the vibration frequency and amplitude. The results in Table 11 show that the control algorithms do not affect the vibration frequency but significantly reduce the vibration amplitudes.

Table 11. Vibrations during crane's motion stoppage.

Trial	Reference Limit	Stress Limit	Frequency	Amplitude	Amplitude
# 1	0	-	1.95 Hz	18.8 mm	100.0%
# 2	Max. 2.0	-	1.95 Hz	13.3 mm	70.7%
# 3	Max. 2.5	-	1.95 Hz	9.2 mm	48.9%
# 4	0	130 MP	1.95 Hz	13.3 mm	70.7%
# 5	0	110 MP	1.95 Hz	2.5 mm	13.3%
# 6	Max. 1.5	120 MP	1.95 Hz	6.2 mm	33.0%
# 7	Max. 1.5	110 MP	1.95 Hz	3.1 mm	16.5%

According to the obtained results, both developed algorithms notably improved the fatigue life of the boom in laboratory experiments. The orientation feedback control increased the fatigue life by between a few tens of percent and approximately one hundred percent. Superior results were obtained with the stress feedback control, which led to increases in fatigue life of several hundred percent. The substantial increase in fatigue life is attributed to the ability of the control algorithms to dampen vibrations, thereby reducing the vibration-induced stresses that drive fatigue.

The most significant difference between the crane's behavior in the laboratory tests and in the simulation model was the damping of vibrations. This was also evident from a comparison of the simulated and measured stress histories.

7. Conclusions

The aim of this study was to improve the fatigue life of a hydraulic crane subjected to significant fatigue-inducing loads through intelligent stress mapping and control, while minimizing undesirable changes in the machine's dynamic behavior. The crane was modelled and co-simulation between ADAMS and MATLAB was performed. The flexibility model of the boom was created in ANSYS in the first method and assessed directly within ADAMS in the second. The maximum principal and von Mises hot spot stress methods were used to determine the highest stresses in the simulation. Because the boom is made of steel, the maximum von Mises stress was selected for the stress optimization process using a neural network (NN). The comparative analysis showed that the neural network model achieved notably higher accuracy for predicting the stresses on the boom than the co-simulation. In addition, two control algorithms were developed, and the system performance was examined through simulation during a short operation cycle involving routine crane movements. The first algorithm was based on a neural network, which optimized the crane's motion according to its orientation and reduced the motion speeds at critical positions, thereby decreasing the peak stresses and increasing the fatigue life; however, statistical effects were not considered at this stage. The second control algorithm was based on fuzzy logic: the stress state of the lifting boom was measured using strain gauges, and when the stress values approached the predefined threshold, the fuzzy logic controller acted to restore the stress state to a satisfactory level. The stress feedback control algorithm also achieved promising results through simulation, displaying a damping effect on crane vibrations. The simulation models of the control algorithms were also integrated into the control system of the prototype crane in the laboratory, and operation cycles were performed on the prototype while accounting for statistical factors such as the distribution of working movements within the operational range. In laboratory experiments, the fatigue life of the boom was significantly improved with the developed control algorithms, ranging from a few percent to several hundred percent.

This study presents a unique contribution by integrating stress mapping with AI-driven control strategies in hydraulic cranes, combining Neural Networks and Fuzzy Logic to optimize stress distribution and reduce fatigue. The experimental validation on a prototype crane demonstrates the practical applicability of the approach and represents a step forward in the use of intelligent control systems for structural durability and efficiency. A direction for future research is to incorporate the crane's other motions, such as rotation and telescoping, in addition to the regular movements.

It should be noted that the reported fatigue-life values are estimates obtained for the specific operation cycle and load case considered. They were derived from the constant-amplitude equivalent stress ranges extracted from the stress histories using the rainflow method and compared against the FAT 103 detail category and the SFS 2378 nominal-stress curve, and they depend on the assumed S–N detail category, the stress-concentration assumptions at the welded pipe fixture, and the accuracy of the strain-gauge and co-simulation stress data. The values should therefore be interpreted as relative comparisons between the controlled and uncontrolled cases rather than as absolute service-life predictions.

The proposed stress-mapping and control framework is general and can, in principle, be applied to other crane configurations and hydraulic drive types, since it relies on a co-simulation and identification procedure together with stress feedback rather than on a fixed plant model. Its accuracy and effectiveness, however, depend on the specific valve dynamics, actuation mechanism, and operating conditions; for a different system, the simulation model would need to be re-identified and the controller re-tuned, and additional experimental validation would be required.

Author Contributions: Conceptualization, D.R.; Methodology, D.R.; Software, A.-O.A. and S.M.; Validation, D.R.; Formal analysis, S.M.; Investigation, D.R.; Resources, D.R.; Data curation, A.-O.A. and S.M.; Writing—original draft, A.-O.A. and S.M.; Writing—review & editing, A.-O.A.; Visualization, A.-O.A. and S.M.; Supervision, D.R.; Project administration, D.R. All authors have read and agreed to the published version of the manuscript.

Funding: This research received no external funding.

Data Availability Statement: The data presented in this study are available on request from the corresponding author.

Conflicts of Interest: The authors have no relevant financial or non-financial interests to disclose.

References

1. Do, T.C.; Dang, T.D.; Dinh, T.Q.; Ahn, K.K. Developments in energy regeneration technologies for hydraulic excavators: A review. *Renew. Sustain. Energy Rev.* **2021**, *145*, 111076. https://doi.org/10.1016/j.rser.2021.111076.
2. Dong, Q.; Xu, G.N.; Ren, H.L.; Wang, A.H. Fatigue remaining life estimation for remanufacturing truck crane jib structure based on random load spectrum. *Fatigue Fract. Eng. Mater. Struct.* **2016**, *40*, 706–731. https://doi.org/10.1111/ffe.12540.

3. Shevchuk, D.; Malysheva, I.; Alizadeh, M.; Handroos, H. Simulated and experimental analysis of a log crane with conventional and direct-driven hydraulics. In Proceedings of the ASME/BATH 2021 Symposium on Fluid Power and Motion Control, Virtual, 19–21 October 2021; p. V001T01A044. https://doi.org/10.1115/FPMC2021-68939.
4. Buczkowski, R.; Żyliński, B. Finite element fatigue analysis of unsupported crane. *Pol. Marit. Res.* **2021**, *28*, 127–135. https://doi.org/10.2478/pomr-2021-0012.
5. Lagerev, A.V.; Lagerev, I.A. Dynamic processes of loader cranes manipulators with excessive backlashes and elastic damping in their hinges. Period. Polytech. Mech. Eng. 2020, 64, 7–14. https://doi.org/10.3311/PPme.12831.
6. Potakhov, E.A. Dynamic loads on a hydraulic cylinder adjusting a crane jib. *Russ. Eng. Res.* **2022**, *42*, 23–29. https://doi.org/10.3103/S1068798X22010178.
7. Chu, Y.; Æsøy, V.; Ehlers, S.; Zhang, H. Integrated multi-domain system modelling and simulation for offshore crane operations. *Ship Technol. Res.* **2015**, *62*, 36–46. https://doi.org/10.1179/0937725515Z.0000000004.
8. Komarov, T.; Zhidchenko, V.; Alizadeh, M.; Handroos, H. Open-loop coordinated tip control of a log crane with and without counterbalance valves. In Proceedings of the 18th Scandinavian International Conference on Fluid Power (SICFP'23), Tampere, Finland, 30 May–1 June 2023.
9. Mattila, J.; Koivumäki, J.; Caldwell, D.G.; Semini, C. A survey on control of hydraulic robotic manipulators with projection to future trends. *IEEE/ASME Trans. Mechatron.* **2017**, *22*, 669–680. https://doi.org/10.1109/TMECH.2017.2668604.
10. Roozbahani, H.; Alizadeh, M.; Ahomäki, A.; Handroos, H. Coordinate-based control for materials handling equipment utilizing real-time simulation. *Autom. Constr.* **2021**, *122*, 103483. https://doi.org/10.1016/j.autcon.2020.103483.
11. Jensen, K.J.; Ebbesen, M.K.; Hansen, M.R. Online deflection compensation of a flexible hydraulic loader crane using neural networks and pressure feedback. *Robotics* **2022**, *11*, 34. https://doi.org/10.3390/robotics11020034.
12. Tuan, L.A.; Cuong, H.; Pham, V.T.; Cong, N.L.; Duc, V.; Le, V.-A. Adaptive neural network sliding mode control of shipboard container cranes considering actuator backlash. *Mech. Syst. Signal Process.* **2018**, *112*, 233–250. https://doi.org/10.1016/j.ymssp.2018.04.030.
13. Hao, W.; Kan, J. Application of self-tuning fuzzy proportional-integral-derivative control in hydraulic crane control systems. *Adv. Mech. Eng.* **2016**, *8*, 1687814016655258. https://doi.org/10.1177/1687814016655258.
14. Seo, J.; Cha, M.; Oh, K.; Park, Y.J. Development of steering control algorithms with self-tuning fuzzy PID for all-terrain cranes. In Proceedings of the 20th International Conference on Control, Automation and Systems (ICCAS), Busan, Republic of Korea, 13–16 October 2020; pp. 727–730. https://doi.org/10.23919/ICCAS50221.2020.9268346.
15. Wonohadidjojo, D.M.; Kothapalli, G.; Hassan, M.Y. Position control of electro-hydraulic actuator system using fuzzy logic controller optimized by particle swarm optimization. *Int. J. Autom. Comput.* **2013**, *10*, 181–193. https://doi.org/10.1007/s11633-013-0711-3.
16. Mikkola, A. Using the simulation model for identification of the fatigue parameters of hydraulically driven log crane. *ASME J. Mech. Des.* **2001**, *123*, 125–131. https://doi.org/10.1115/1.1343110.
17. Pedersen, M.M. Improving the Fatigue and Control Performance of Loader Cranes; Special Report No. 71; Department of Mechanical Engineering, Aalborg University: Aalborg East, Denmark, 2011.
18. Zhidchenko, V.; Handroos, H.; Kovartsev, A. Application of digital twin and IoT concepts for solving the tasks of hydraulically actuated heavy equipment lifecycle management. *Int. J. Eng. Syst. Model. Simul.* **2020**, *11*, 194–206. https://doi.org/10.1504/IJESMS.2020.111277.
19. Zhao, G.; Xiao, J.; Zhou, Q. Fatigue models based on real load spectra and corrected S-N curve for estimating the residual service life of the remanufactured excavator beam. *Metals* **2021**, *11*, 365. https://doi.org/10.3390/met11020365.
20. Hectors, K.; Chaudhuri, S.; De Waele, W. Fracture mechanics and hot spot stress-based fatigue life calculation: Case study for a crane runway girder. *Fatigue Fract. Eng. Mater. Struct.* **2022**, *45*, 2662–2675. https://doi.org/10.1111/ffe.13729.
21. Li, C.; Qi, Q.; Dong, Q.; Yu, Y.; Fan, Y. Research on fatigue remaining life of structures for a dynamic lifting process of a bridge crane. *J. Mech. Sci. Technol.* **2023**, *37*, 1789–1801. https://doi.org/10.1007/s12206-023-0319-7.
22. Yang, X.; Ge, Y.; Zhu, W.; Deng, W.; Zhao, X.; Yao, J. Adaptive Motion Control for Electro-hydraulic Servo Systems with Appointed-Time Performance. *IEEE/ASME Trans. Mechatron.* **2025**, *30*, 7009–7018. https://doi.org/10.1109/TMECH.2024.3525013.
23. Yang, X.; Deng, W.; Yao, J. Neural Adaptive Dynamic Surface Asymptotic Tracking Control of Hydraulic Manipulators with Guaranteed Transient Performance. *IEEE Trans. Neural Netw. Learn. Syst.* **2023**, *34*, 7339–7349. https://doi.org/10.1109/TNNLS.2022.3141463.

24. Kotta, J. Modeling of PATU-655 Loader with a Combination of Mevea and Simulink Using Functional Mock-Up Interface. Master's Thesis, Department of Mechanical Engineering, Lappeenranta-Lahti University of Technology, Lappeenranta, Finland, 2021.
25. Ángel, L.; Pérez, M.P.; Díaz-Quintero, C.; Mendoza, C. ADAMS/MATLAB co-simulation: Dynamic systems analysis and control tool. *Appl. Mech. Mater.* **2012**, *232*, 527–531. https://doi.org/10.4028/www.scientific.net/AMM.232.527.
26. Sosa-Méndez, D.; Lugo-González, E.; Arias-Montiel, M.; García-García, R.A. ADAMS-MATLAB co-simulation for kinematics, dynamics, and control of the Stewart–Gough platform. *Int. J. Adv. Robot. Syst.* **2017**, *14*, 172988141771982. https://doi.org/10.1177/1729881417719824.
27. Agyemang, A.O. Intelligent Mapping of Stresses in a Hydraulic Crane. Master's Thesis, Department of Mechanical Engineering, Lappeenranta-Lahti University of Technology, Lappeenranta, Finland, 2014.
28. Li, W.; Zhao, J.; Jiang, Z.; Chen, W.; Zhou, Q. A numerical study of the overall stability of flexible giant crane booms. *J. Constr. Steel Res.* **2015**, *105*, 12–27. https://doi.org/10.1016/j.jcsr.2014.10.006.
29. Trąbka, A. Influence of flexibilities of cranes structural components on load trajectory. *J. Mech. Sci. Technol.* **2016**, *30*, 1–14. https://doi.org/10.1007/s12206-015-1201-z.
30. Krukowski, J.; Maczyński, A. Application of the rigid finite element method for modelling an offshore pedestal crane. *Arch. Mech. Eng.* **2013**, *LX*, 3. https://doi.org/10.2478/meceng-2013-0028.
31. Zhang, X.X.; Sun, C.S.; Zhu, J.H.; Yang, X.F. Finite element analysis on flexible attachments of luffing jib tower crane. *Adv. Mater. Res.* **2010**, *118–120*, 512–516. https://doi.org/10.4028/www.scientific.net/AMR.118-120.512.
32. Seo, J.K.; Kim, M.H.; Shin, S.B.; Han, M.S.; Park, J.S.; Mahendr, M.; Lee, J.M. Comparison of hot spot stress evaluation methods for welded structures. *Int. J. Nav. Archit. Ocean Eng.* **2010**, *2*, 200–214. https://doi.org/10.3744/jnaoe.2010.2.4.200.
33. Wang, B.J.; Li, Q.; Liu, Z.M. Study of typical welded joint hot spot stress concentration factor. *Adv. Mater. Res.* **2010**, *160–162*, 1482–1487. https://doi.org/10.4028/www.scientific.net/amr.160-162.1482.
34. SFS-ENV 1993-1-1. Eurocode 3: Design of Steel Structures, Part 1-1: General Rules and Rules for Buildings; Finnish Standards Association (SFS): Helsinki, Finland, 1993.
35. Machado, I.C.V.; Viana, H.F.; da Silva, R.G.L.; Costa, R.S.; Lavall, A.C.C. Finite element model for advanced analysis of plane steel frames with hinged end conditions including von Mises criterion. *Structures* **2022**, *46*, 1918–1937. https://doi.org/10.1016/j.istruc.2022.10.116.
36. Yu, J.; Fei, Q.; Zhang, P.; Li, Y.; Zhang, D.; Guo, F. An innovative yield criterion considering strain rates based on von Mises stress. *ASME J. Press. Vessel. Technol.* **2020**, *142*, 014501. https://doi.org/10.1115/1.4044908.
37. Mäkinen, S. Älykkäiden Ohjausjärjestelmien Käyttö Puutavarakuormaimen Väsymiskestoiän Parantamisessa. Master's Thesis, Department of Mechanical Engineering, Lappeenranta-Lahti University of Technology, Lappeenranta, Finland, 2001.
38. SFS 2378. Fatigue Design and Load Capacity of Welded Joints in Steel Structures; Finnish Standards Association (SFS): Helsinki, Finland, 1992.